INL/EXT-19-54899

Comparison of Generation of Higher-Order Neutron Scattering Cross Sections

William C. Dawn[1], Javier Ortensi[2], Mark D. DeHart[2], Scott P. Palmtag[1]

[1] Department of Nuclear Engineering
North Carolina State University
Raleigh, NC, USA 27695-7909

[2] Reactor Physics Design and Analysis Department
Idaho National Laboratory
P.O. Box 1625
Idaho Falls, ID 83415-3870

January 2020

INL is a U.S. Department of Energy National Laboratory operated by Battelle Energy Alliance

DISCLAIMER

This material is based upon work supported under an Integrated University Program Graduate Fellowship. Any opinions, findings, conclusions, or recommendations expressed in this publication are those of the author and do not necessarily reflect the views of the Department of Energy Office of Nuclear Energy.

INL/EXT-19-54899

Comparison of Generation of Higher-Order Neutron Scattering Cross Sections

William C. Dawn[1], Javier Ortensi[2], Mark D. Dehart[2], Scott P. Palmtag[1]

January 2020

[1] Department of Nuclear Engineering
North Carolina State University
Raleigh, NC, USA 27695-7909

[2] Reactor Physics Design and Analysis Department
Idaho National Laboratory
Idaho Falls, ID, USA 83415-3870

http://www.inl.gov

Prepared for the
U.S. Department of Energy
Office of Nuclear Energy
Under DOE Idaho Operations Office
Contract DE-AC07-05ID14517

Abstract

The generation of high scattering order neutron scattering cross sections consistent with high-fidelity simulations remains an area of active research. Popular options include generating cross sections from continuous energy Monte Carlo calculations or from a deterministic neutron transport calculation with high-fidelity tabulated cross sections. Both options present challenges.

Monte Carlo simulations can naturally process continuous energy cross-section data and allow for the general description of anisotropic neutron scattering given a scattering law. However, Monte Carlo simulations are inherently related to particle weighting and it has been suggested that this may be unacceptable for generating high-order neutron scattering cross sections. Deterministic neutron transport calculations can easily calculate high-order moments of the flux to appropriately calculate higher-order neutron scattering cross sections but are generally limited by discretization of space, energy, and angle.

In this work, the trade-offs between generation of high-order neutron scattering cross sections via Monte Carlo and deterministic neutron transport methods are investigated. The methods implemented in the Monte Carlo computer program Serpent 2 and the deterministic fast reactor neutron cross section generator MC^2-3 are compared. Cross sections resulting from these methods are used in Rattlesnake, a deterministic neutron transport code developed by Idaho National Laboratory, and results are compared to a reference continuous energy Monte Carlo calculation.

Whereas previous work investigating the effects of anisotropic neutron scattering has focused on light water reactor simulations, this work focuses on high-order neutron scattering cross sections as they relate to fast reactor simulations. To investigate the consequences of the Serpent 2 and MC^2-3 methodologies, a test problem is developed. The test problem is a one-dimensional geometry with fast reactor materials designed to demonstrate deep penetration and exacerbate the effects of high-order neutron scattering.

Based on the results of the deep penetration test problem, it is concluded that P_3 neutron scattering cross sections are sufficient to describe anisotropic scattering in fast reactor materials. Any neutron scattering of order higher than P_3 offers negligible change in the eigenvalue of the test problem. Additionally, it is determined that the methodology as implemented in Serpent 2 is applicable for generating high-order neutron scattering cross sections through at least P_3 in fast reactor materials.

Contents

1 Introduction **1**

2 Theory **2**
2.1 Nature of Anisotropic Neutron Scattering 2
2.2 Numerical Treatment of Anisotropic Neutron Scattering 2

3 Comparison of Methodologies **5**
3.1 MC^2-3 Methodology 5
3.2 Serpent 2 Methodology 7

4 Results **9**
4.1 Test Problem Description 9
4.2 Monte Carlo Results 10
4.3 Rattlesnake Comparison Results 11

5 Conclusions **15**
5.1 Future Work 15

Acronyms **18**

References **19**

A Material Compositions **21**

List of Figures

1 Ultrafine Group (UFG) to Broad Group (BG) Group Condensation in MC^2-3 Using Two-Dimensional Transport Solutions [1]. 6
2 Description of Test Geometry. 10
3 Flux Spectra from Continuous Energy Serpent 2 Model. 11
4 Flux Profile in Test Problem from Serpent 2 Model, Cutoff Energy 1 keV. . 12
5 Spatial and Angular Refinement Study. 13

List of Tables

1 Eigenvalue Results from Rattlesnake using Serpent 2 and MC^2-3 Cross Sections. 14
A.1 Fuel Material Number Densities for U-10Zr with 10 wt.% ^{235}U. 21
A.2 Sodium Material Number Density. 21
A.3 HT9 Stainless Steel Material Number Densities. 22

1 Introduction

While modern computers allow for continuous energy Monte Carlo neutron transport calculations, reduced-order models remain popular. Multigroup neutron transport and multigroup neutron diffusion simulations are commonly used in transient, coupled multiphysics, and optimization calculations where high-fidelity models remain computationally prohibitive. However, these reduced-order models require data, such as multigroup cross sections, that are problem specific. Therefore, a method for generating multigroup cross sections for use in reduced-order simulations that is consistent with high-fidelity simulations remains an area of active research.

For reduced-order simulations, material cross sections must be discretized in space, energy, and angle. Discretization in space and energy is often straightforward and relies on grid-based techniques. However, discretization in angle is often more challenging. The angular dependence of multigroup cross sections is often addressed by projecting the continuous form of the neutron scattering cross section given by a scattering law onto Legendre polynomials. It is precisely this projection of the multigroup neutron scattering cross section onto Legendre polynomials of that is investigated here.

A variety of methods have been developed for the generation of high-order neutron scattering cross sections using both deterministic and Monte Carlo techniques [1–4]. In this work, the theory of projecting the multigroup neutron scattering cross section onto Legendre polynomials is first discussed in Section 2. Then cross section generation methodologies of the fast reactor cross section generator MC^2-3 and the Monte Carlo neutron transport code Serpent 2 are compared in Section 3. Results are presented based on multigroup cross sections generated from MC^2-3 and Serpent 2 in Section 4. Finally, conclusions are made in Section 5 based on the comparison of the methods and their respective results.

2 Theory

To understand the importance and proper treatment of anisotropic neutron scattering, the underlying phenomena must be understood. Based on this understanding, numerical treatments may be derived. The following subsections discuss the nature and numerical representation of neutron scattering anisotropy.

2.1 Nature of Anisotropic Neutron Scattering

In this work, anisotropy in the neutron scattering cross section is due solely to material properties. That is, the angular dependence of the neutron scattering cross section is treated as a property of an isotope and is attributable to physical laws. It can be demonstrated that isotopes with low atomic mass will cause the greatest degree of anisotropic neutron scattering [5]. This is known to be a significant challenge in light water reactor (LWR) simulations where the coolant/moderator contains a significant fraction of ^{1}H. However, anisotropic scattering in materials common to fast reactors has not been investigated as extensively [6]. It is also known that anisotropic neutron scattering has strong dependence on incident neutron energy and therefore the effect of anisotropic neutron scattering may be compounded in fast reactor systems.

Alternatively, the angular dependence of the neutron scattering cross section could be used to describe macroscopic neutron transport behavior. For example, using an equivalence technique similar to SuPer Homogenization (SPH), one could develop a method by which neutron streaming effects were described by an angularly dependent neutron scattering cross section [7, 8]. Such a method would allow for the preservation of neutron streaming typically lost during spatial homogenization. However, this method is not considered here and all models considered have their geometries represented exactly without spatial homogenization.

2.2 Numerical Treatment of Anisotropic Neutron Scattering

Attention will be focused on the discretization of the angular dependence of the neutron flux and the doubly-differential neutron scattering cross section. Allow $\Psi(\mathbf{r}, E, \widehat{\Omega})$ to be the continuous form of the neutron flux at spatial position $\mathbf{r}$ with energy E and direction $\widehat{\Omega}$. The

flux can then be projected onto spherical harmonics functions, $Y^{m,n}(\widehat{\Omega})$, as

$$\Psi(\mathbf{r},E,\widehat{\Omega}) = \sum_{n=0}^{\infty} \frac{2n+1}{2} \sum_{m=-n}^{n} \Psi^{m,n}(\mathbf{r},E)\, Y^{m,n}(\widehat{\Omega}) \tag{1}$$

where $\Psi^{m,n}(\mathbf{r},E)$ are the coefficients of the expansion that satisfy the relationship

$$\Psi^{m,n}(\mathbf{r},E) = \int_{4\pi} \Psi(\mathbf{r},E,\widehat{\Omega})\, Y^{m,n}(\widehat{\Omega})\, d\widehat{\Omega}. \tag{2}$$

The expansion coefficients, $\Psi^{m,n}(\mathbf{r},E)$, are also termed the moments of the flux. Note that in practice, the infinite series in Eq. (1) will be truncated at some finite order such that $n = 1,\ldots,N$.

For the angular dependence of the neutron scattering cross section, allow

$$\Sigma_s(\mathbf{r},E' \rightarrow E, \widehat{\Omega}' \rightarrow \widehat{\Omega})$$

to be the doubly-differential neutron scattering cross section at spatial position $\mathbf{r}$ for neutrons scattering from energy E' to energy E and from direction $\widehat{\Omega}'$ to direction $\widehat{\Omega}$. Then the neutron scattering cross section can be written in terms of the cosine of the scattering angle, $\mu_0 = \widehat{\Omega}' \cdot \widehat{\Omega}$, as $\Sigma_s(\mathbf{r},E' \rightarrow E, \mu_0)$.

The angular dependence of the scattering cross section can be projected onto the set of Legendre polynomials as

$$\Sigma_s(\mathbf{r},E' \rightarrow E, \mu_0) = \sum_{n=0}^{\infty} \frac{2n+1}{2} \Sigma_s^n(\mathbf{r},E' \rightarrow E)\, P_n(\mu_0) \tag{3}$$

where $P_n(\mu_0)$ are the Legendre polynomials and $\Sigma_s^n(\mathbf{r},E' \rightarrow E)$ are the expansion coefficients such that

$$\Sigma_s^n(\mathbf{r},E' \rightarrow E) = \int_{-1}^{1} \Sigma_s(\mathbf{r},E' \rightarrow E, \mu_0)\, P_n(\mu_0)\, d\mu_0. \tag{4}$$

Similar to the terminology for the moments of the flux, the Legendre expansion coefficients in Eq. (3) are termed the moments of the neutron scattering cross section. For $n > 0$, $\Sigma_s^n(\mathbf{r},E' \rightarrow E)$ is also known as a higher-order neutron scattering cross section.

In the transition from high-order models, where $\Sigma_s(\mathbf{r},E' \rightarrow E, \widehat{\Omega}' \rightarrow \widehat{\Omega})$ is treated explicitly using a scattering law, to reduced-order models, the moments of the neutron scattering cross section must be obtained. There are two general methods for calculating $\Sigma_s^n(\mathbf{r},E' \rightarrow E)$. First, the scattering probability distribution function, $f(\mathbf{r},\mu_0,E')$, can be estimated and

used to calculate the expansion coefficients using ENDF data. Alternatively, the expansion coefficients themselves can be estimated using Eq. (4).

Both methods for estimating $f(\mathbf{r},\mu_0,E')$ and directly estimating $\Sigma_s^n(\mathbf{r},E'\rightarrow E)$ have been implemented in Monte Carlo methods [4]. In deterministic calculations, estimating $f(\mathbf{r},\mu_0,E')$ is not possible as the scattering function typically requires a tallying procedure to estimate. However, in deterministic calculations, the moments of the neutron flux can be calculated directly, which helps to simplify the calculation in Eq. (4). It is worth noting that the ENDF file format uses the form of

$$f(\mu_0,E') = \sum_{n=0}^{N} \frac{2n+1}{2} a_n(E')\, P_n(\mu_0) \tag{5}$$

where the scattering function is a function of both neutron scattering angle, μ_0, and incident neutron energy E'. The spatial dependence of the scattering function in Eq. (5) has been suppressed as ENDF data is isotopic data for general geometries. In the ENDF data structure, Legendre polynomial expansion coefficients, $a_n(E')$, are stored [9].

3 Comparison of Methodologies

The generation higher-order neutron scattering cross sections is investigated in computer programs applicable to fast reactors. Deterministic computer programs such as MC^2-3 and CENTRM have the ability to generate appropriately weighted higher-order neutron scattering cross sections for fast systems [1, 10]; Monte Carlo computer programs such as Serpent 2 and MCNP can also perform similar functions [11, 12]. In the present study, MC^2-3 and Serpent 2 are considered.

3.1 MC^2-3 Methodology

MC^2-3 is a multigroup cross section generation code for fast reactor analysis developed by Argonne National Laboratory (ANL) [1]. While newer versions of the computer program may provide capabilities for simplified geometric models, these are not typically used in practice. Instead, MC^2-3 is used for cross section condensation in infinite homogeneous media and is coupled to TWODANT, which solves the discrete ordinates neutron transport equations [13]. The TWODANT solution is then used to calculate the moments of the flux, $\Psi^{m,n}(\mathbf{r},E)$, from Eq. (1) for simplified, two-dimensional geometries. The typical flow of calculations as described in the MC^2-3 User's Manual is provided in Fig. 1.

The cross section generation process begins with the calculation of the moments of the flux using the discrete ordinates solution from TWODANT and the MC^2-3 Ultrafine Group (UFG) energy structure (2,082 groups). The flux moments from TWODANT are then used to perform the group condensation from the UFG structure to an arbitrary user-specified Broad Group (BG) structure (typically 33 groups). Given the moments of the flux from Eq. (1), the group condensation of the moments of the neutron scattering cross section can be expressed as

$$\Sigma^n_{G'\rightarrow G}(\widehat{\Omega}) = \frac{\sum_{g\in G}\sum_{g'\in G'}\Sigma^n_{g'\rightarrow g}(\sum^n_{m=-n}\Psi^{m,n}_{g'}Y^{m,n}(\widehat{\Omega}))}{\sum^n_{m=-n}\Psi^{m,n}_{G'}Y^{m,n}(\widehat{\Omega})} \tag{6}$$

where g is the UFG index, G is the BG index, and the notation $g \in G$ implies the summation over all UFGs that are contained within the G^{th} BG. In Eq. (6) the dependence on spatial position, $\mathbf{r}$, has been suppressed as the group condensation in MC^2-3 is performed in an infinite-homogeneous medium using the flux moments spectra from TWODANT. Note that the denominator of Eq. (6) is the multigroup neutron flux moment that has been condensed

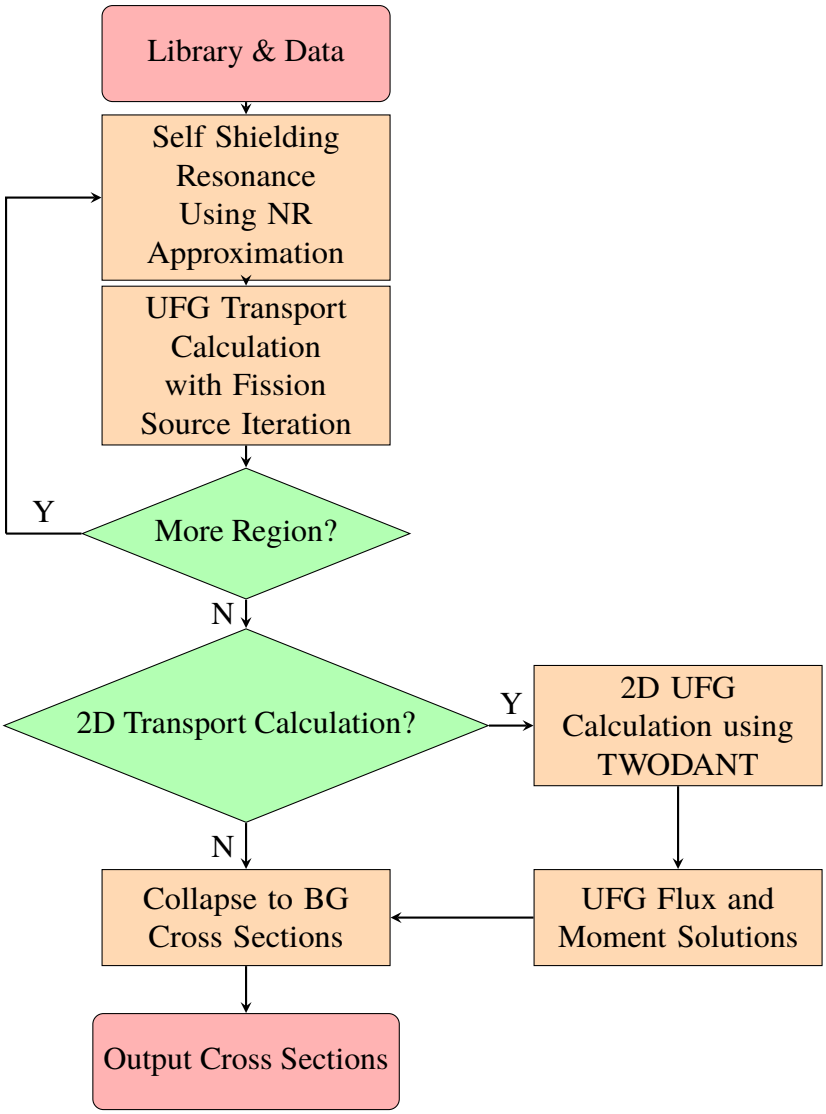

Figure 1: Ultrafine Group (UFG) to Broad Group (BG) Group Condensation in MC^2-3 Using Two-Dimensional Transport Solutions [1].

as

$$\Psi_G^{m,n} = \sum_{g \in G} \Psi_g^{m,n}. \tag{7}$$

The resulting moment of the neutron scattering cross section in Eq. (6) is angularly dependent, which is undesirable. As such, the group condensation is performed with the flux moments as

$$\Sigma_{G' \to G}^{m,n} = \frac{\sum_{g \in G} \sum_{g' \in G} \Sigma_{g' \to g}^{n} \Psi_{g'}^{m,n}}{\Psi_{G'}^{m,n}} \tag{8}$$

where the resulting $\Sigma_{G' \to G}^{m,n}$ is no longer dependent on angle but is now dependent on the spherical harmonics rather than Legendre polynomials. However, as

$$m = -n, -n+1, \ldots, 0, \ldots, n-1, n$$

there are $2n+1$ possible combinations for the expression of Eq. (8). In the MC^2-3 implementation, all moments of the flux are weighted equally as

$$\Sigma_{G' \to G}^{n} = \frac{\sum_{g \in G} \sum_{g' \in G'} \Sigma_{g' \to g}^{n} (\sum_{m=-n}^{n} \left| \Psi_{g'}^{n,m} \right|)}{\sum_{g' \in G'} (\sum_{m=-n}^{n} \left| \Psi_{g'}^{n,m} \right|)} \tag{9}$$

where $|\cdot|$ represents the absolute value and is necessary as the higher-order moments of the flux may be negative.

The implementation in MC^2-3 as in equation Eq. (9) is promising as it contains information from all available moments of the flux. However, the quality of the MC^2-3 formulation is directly related to the accuracy of the moments of the flux as calculated by TWODANT. This requirement of using TWODANT is quite strict as the computer program only supports simplified, two-dimensional geometries. In reactor applications, this often results in approximating a sodium-cooled fast reactor (SFR) with hexagonal geometry in a cylindrical, r-z model. While the angular dependence of the moments of the neutron scattering cross section is treated well, the restrictive geometric descriptions available in TWODANT may be a poor approximation.

3.2 Serpent 2 Methodology

Calculation of multigroup scattering moments of neutron scattering cross sections via Monte Carlo techniques is notoriously difficult. As shown in the MC^2-3 methodology from Eq. (9),

the multigroup condensation of the neutron scattering moments should be weighted with the energy spectra of the moments of the flux. However, moments of the flux are typically not available in Monte Carlo calculations. It has been suggested that if the neutron current (first moment) were tallied using a Monte Carlo technique, statistical convergence would be challenging due to the high degree of symmetry in nuclear reactor geometries [2]. Naturally, Monte Carlo calculations and tallying particle weights are inherently related to the scalar flux (zeroth moment) and this presents an open challenge for the generation of higher-order moments of the neutron scattering cross section using such methods. The potential problem of performing the calculation of the moments of the scattering cross section using the scalar flux is that the energy spectra of higher-order moments need not be closely related to the energy spectrum of the scalar flux. However, it has been demonstrated elsewhere that these energy spectra are typically similar for LWR simulations [4].

Redmond implemented a method to calculate higher-order neutron scattering moments using the scalar flux as calculated in the computer program MCNP-4C [4]. The method proposed by Redmond can be written

$$\Sigma^n_{s,G'\to G} = \frac{\int_{-1}^{1} \left(\int_{E_G}^{E_{G+1}} \int_{E_{G'}}^{E_{G'+1}} \int_{\Delta V} \phi(\mathbf{r},E') \Sigma_s(\mathbf{r},E') f(E'\to E,\mu_0)\, d\mathbf{r}\, dE'\, dE \right) P_n(\mu_0)\, d\mu_0}{\int_{E_{G'}}^{E_{G'+1}} \int_{\Delta V} \phi(\mathbf{r},E')\, d\mathbf{r}\, dE'} \tag{10}$$

where $\phi(\mathbf{r},E)$ is the scalar flux and ΔV is a volume within the calculation domain.

While Eq. (10) does use the energy spectrum associated with the scalar flux rather than higher-order moments of the flux, the implementation was validated in a series of three test problems designed to simulate LWR conditions [4]. It was demonstrated that the calculation of higher-order neutron scattering cross sections as in Eq. (10) provided consistent results between Monte Carlo and deterministic transport calculations. In the test problems, scattering moments were calculated for $n = \{0,1,3,5,7\}$ and accuracy improved significantly with increasing scattering order, n, until $n = 3$, at which point any additional improvements were negligible. However, these test problems all contained significant fractions of ^{1}H (up to 98 at.%) which is known to demonstrate significant anisotropic neutron scattering. The results of Redmond may not extend to fast reactor materials or geometries.

The calculation of higher-order scattering moments in Serpent 2 is implemented in a method similar to Eq. (10) [11, 14]. Concern has been expressed with this implementation due to the dependence on the scalar flux [2]. Additionally, the implementation in Serpent 2 has not been verified in previous literature. This work seeks to address the calculation of higher-order scattering moments using Serpent 2.

4 Results

A test problem is developed to compare the methodologies for generating higher-order moments of the neutron scattering cross section techniques in MC^2-3 and Serpent 2. The test problem is then evaluated in Rattlesnake, a deterministic, neutral particle transport code developed at Idaho National Laboratory (INL) [15]. With Rattlesnake, the test problem is evaluated using higher-order neutron scattering cross sections generated from both MC^2-3 and Serpent 2 for P_n scattering order $n = \{0, 1, 3, 5, 7\}$. All cross sections are based on ENDF/B-VII.0 data as this is the most up-to-date cross section library available in MC^2-3 [1]. Additionally, the "ANL33" 33-group energy structure common to fast reactor analysis and implemented in MC^2-3 is selected for the generation of multigroup cross sections.

4.1 Test Problem Description

To demonstrate the effects of higher-order neutron scattering cross sections, a one-dimensional test problem was designed to exacerbate the effects of anisotropic neutron scattering with materials common to SFR designs. The materials selected are metallic uranium enriched to 10 wt.% ^{235}U alloyed with 10 wt.% zirconium (U-10Zr), metallic sodium, and HT9 stainless steel [16, 17]. Number densities for these materials are provided in Tables A.1, A.2, and A.3 respectively.

Previous literature has demonstrated that "deep penetration" of fast neutrons can exacerbate the effects of anisotropic neutron scattering due to the highly anisotropic neutron flux [18, 19]. Such deep penetration is desirable for comparison of methodologies for the generation of higher-order neutron scattering cross sections. A geometry demonstrating deep penetration is one in which fast neutrons are adjacent to a highly streaming medium such as air. The large neutron mean-free-path through such a medium results in a strong angular dependence of the neutron flux. To compare the methodologies of MC^2-3 and Serpent 2, a one-dimensional test problem has been developed that demonstrates deep penetration, as shown in Fig. 2. The fuel region is adjacent to a large sodium region which is nearly transparent to neutrons at fast energies. Deep penetration is observed within the large steel region near the problem boundary as many mean-free-paths of steel are included.

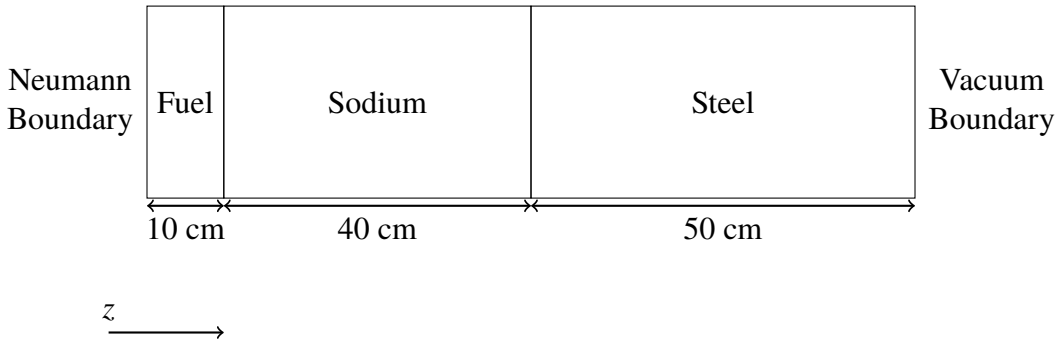

Figure 2: Description of Test Geometry.

A Neumann boundary condition is applied at the left of the problem ($z = 0$ cm) as

$$\begin{aligned} \Psi(0 \text{ cm}, E, \mu_{in}) &= \Psi(0 \text{ cm}, E, \mu_{out}), \quad \text{for} \\ \mu_{in} &= \{\mu \mid \mu > 0\}, \\ \mu_{out} &= \{\mu \mid \mu < 0\}, \end{aligned} \tag{11}$$

where $\mu \equiv \cos\theta$ is the cosine of the polar angle and this simplification is possible due to the choice of one-dimensional geometry. A vacuum boundary condition is applied at the right of the problem ($z = 100$ cm) as

$$\Psi(100 \text{ cm}, E, \mu) = 0 \quad \text{for} \quad \mu < 0. \tag{12}$$

Due to the large fraction of steel adjacent to the boundary in the test geometry, the results are insensitive to the boundary condition near $z = 100$ cm.

4.2 Monte Carlo Results

Results from the continuous energy Serpent 2 model are presented in Fig. 3 and Fig. 4. In both figures, error bars are negligible compared to line widths. The eigenvalue was determined to be $\lambda = 1.02898 \pm 6.0 \times 10^{-5}$; this is used as a reference value for subsequent comparisons. The flux in the fuel has high mean energy, as may be expected. The flux begins to thermalize in the sodium and the large absorption resonance of ^{23}Na at approximately 1 keV can be observed in Fig. 3. Thermalization then continues in the steel, but flux in the steel is low due to significant absorption.

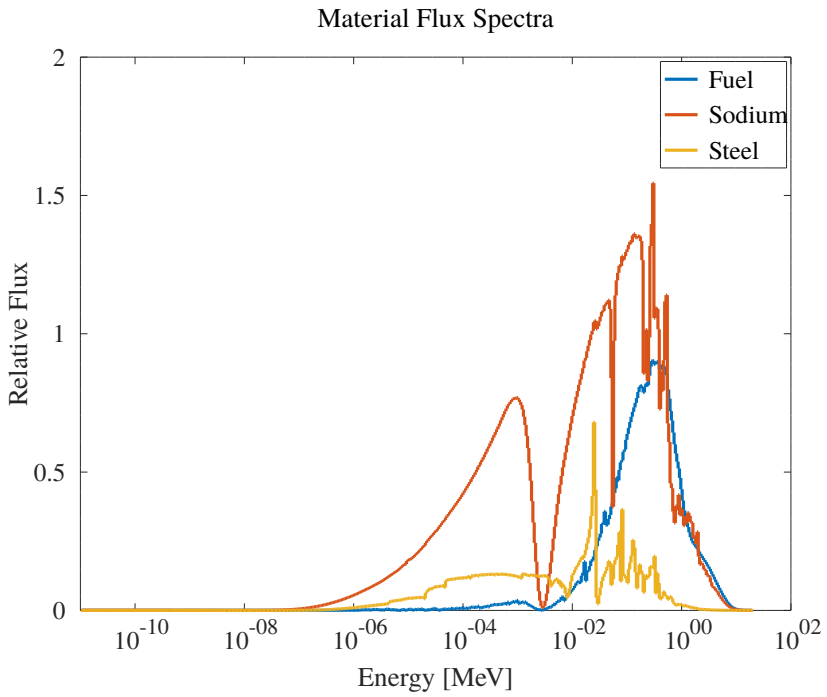

Figure 3: Flux Spectra from Continuous Energy Serpent 2 Model.

The thermalization and scattering can also be observed in Fig. 4. Fast flux peaks in the fuel, thermalization begins in the sodium, and the steel acts as a strong absorber. It is observed in Fig. 4 that the flux is attenuated approximately exponentially in the steel due to absorption.

4.3 Rattlesnake Comparison Results

Multigroup cross sections were generated using both MC^2-3 and Serpent 2 for use in Rattlesnake. In Serpent 2, multigroup macroscopic cross sections were generated by solving the continuous energy neutron transport equation in the exact geometry and tallying neutron interactions and particle weights. In MC^2-3, multigroup microscopic cross sections were generated by solving the multigroup neutron transport equation with 1,042 energy groups, S_8 Gauss-Chebyshev quadrature, and 200 spatial cells to represent the problem geometry. The multigroup microscopic cross sections from MC^2-3 were then mixed within Rattlesnake to calculate macroscopic cross sections. Then both sets of cross sections were used to simulate the test problem described in Section 4.1 using Rattlesnake.

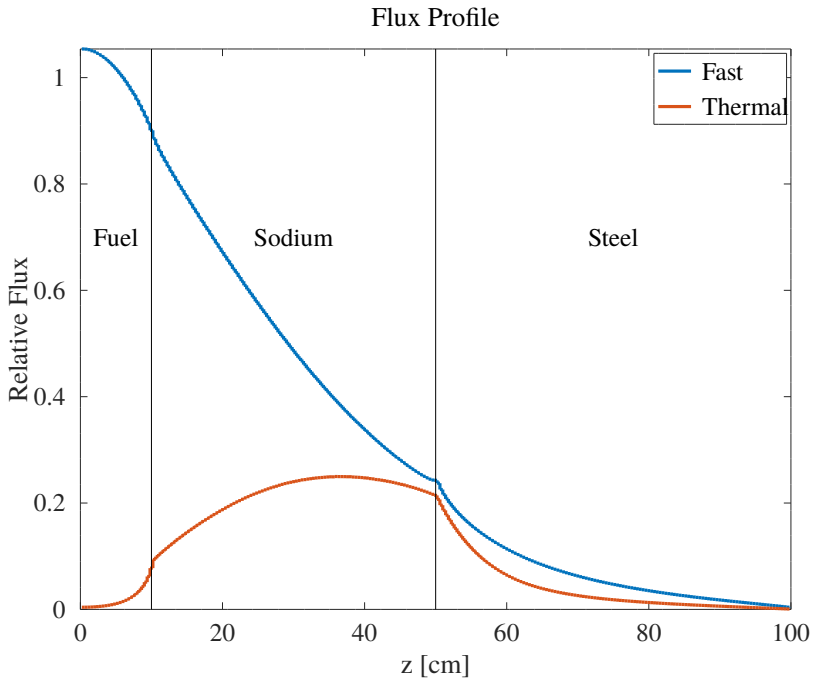

Figure 4: Flux Profile in Test Problem from Serpent 2 Model, Cutoff Energy 1 keV.

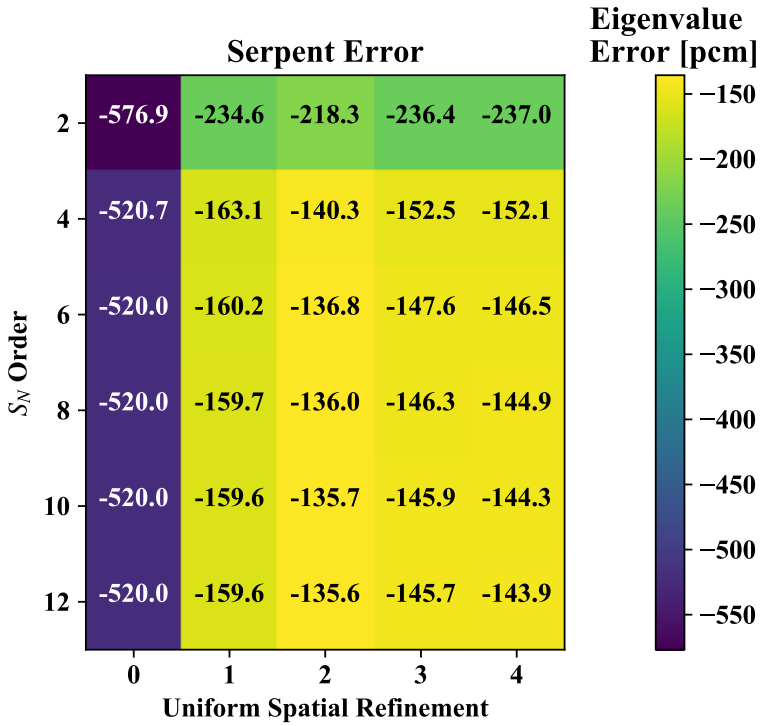

Figure 5: Spatial and Angular Refinement Study.

A preliminary step was to determine the number of spatial elements and number of discrete angles required for a converged model. A refinement study was conducted using Rattlesnake and beginning with 10 elements ($\Delta z = 10$ cm) and S_2 Gauss-Chebyshev quadrature. The Serpent 2 multigroup cross sections were used, the scattering order was held constant at P_7, and the eigenvalue error was measured relative to the continuous energy Monte Carlo result. Results from the refinement study are presented in Fig. 5. The refinement study shows that the multigroup transport solution agrees with the continuous energy Monte Carlo solution to approximately 144 pcm (1 pcm $= 1 \times 10^{-5}$). From the results presented in Fig. 5, it was determined that a spatial refinement of three in Rattlesnake (corresponding to 80 elements and $\Delta z = 1.25$ cm) and S_6 quadrature would be used for all subsequent results. The results in Fig. 5 shows that due to the simplified geometry, the problem converges quickly in space and angle.

After the refinement study, the effects of the higher-order neutron scattering cross sections were investigated. Rattlesnake is used to calculate the eigenvalue in the deep penetration test

Table 1: Eigenvalue Results from Rattlesnake using Serpent 2 and MC^2-3 Cross Sections.

P_n Order	Rattlesnake/Serpent 2	Rattlesnake/Serpent Error pcm	Rattlesnake/MC^2-3	Rattlesnake/MC^2-3 Error pcm
P_0	1.053552	2457.2	1.064405	3542.5
P_1	1.026624	-235.6	1.035212	623.2
P_3	1.027437	-154.3	1.035953	697.3
P_5	1.027453	-152.7	1.035962	698.2
P_7	1.027454	-152.6	1.035964	698.4
Ref.	1.02898 ± 6.0pcm			

problem using cross sections generated with Serpent 2 (Rattlesnake/Serpent) and generated with MC^2-3 (Rattlesnake/MC^2-3). Then the scattering order, n, is varied in Rattlesnake for $n = \{0,1,3,5,7\}$ and the error is computed relative to the continuous energy Monte Carlo results. Results from the scattering order investigation are presented in Table 1.

The results in Table 1 show that agreement in eigenvalue improves with increased scattering order as one may expect. Additionally, these results indicate that P_0 neutron scattering cross sections are unacceptable to describe the angular dependence of neutron scattering in this test problem. Typically, P_0 neutron scattering cross sections would not be used and transport-corrected P_0 (TCP0) cross sections are used instead. The results presented demonstrate that P_1 neutron scattering cross sections significantly improve the agreement of the resulting eigenvalue in the test problem. Table 1 indicates that P_3 neutron scattering cross sections offer additional improvement in the solution. Any neutron scattering of order higher than P_3 represents negligible change in the solution to the deep penetration test problem.

It is observed that the converged Rattlesnake/MC^2-3 results agree to the Monte Carlo Serpent 2 results to approximately 700 pcm. This is acceptable for this test problem but may merit future investigation. It is suggested that this discrepancy is due to the different processing of ENDF/B-VII.0 data in Serpent 2 and MC^2-3. Additional processing steps are required to prepare data for the MC^2-3 UFG libraries and MC^2-3 employs the narrow resonance approximation [1].

In previous literature, a similar study of a one-dimensional geometry with fast reactor materials demonstrated similar results [6]. In the other work, it was observed that the scattering behavior was largely described by P_1 neutron scattering cross sections with small improvement provided by P_3 neutron scattering cross sections.

5 Conclusions

For the deep penetration test problem in Section 4, it has been demonstrated that P_3 neutron scattering cross sections are sufficient for describing the angular dependence of neutron scattering in typical fast reactor materials. Neutron scattering of order higher than P_3 has negligible effect on the results of the deep penetration test problem presented. The convergence of higher-order scattering cross sections generated by both MC^2-3 and Serpent 2 agrees well for increasing scattering order.

Despite concerns expressed in Section 3 regarding the methodology employed in Monte Carlo calculation of higher-order neutron scattering cross sections, the approximation employed in Serpent 2 as in Eq. (10) appears useful for certain simulations. In addition to the LWR test problems demonstrated by Redmond, the deep penetration fast reactor test problem in Section 4 shows satisfactory agreement between the cross section generation methodologies employed in Serpent 2 and MC^2-3. The results of the deep penetration test demonstrated that Serpent 2 can reasonably be used to generate higher-order neutron scattering moments through at least P_3 and for fast reactor materials.

Though the theory supporting the methodology in MC^2-3 is favorable, MC^2-3 is restricted by the requirement of calculating the flux moments using TWODANT. The choice must be made whether the higher-order scattering effects or geometric effects will dominate. For the simplified deep penetration model here, both cross section generation options are satisfactory as TWODANT can exactly represent the geometry. However, for realistic reactor geometries, it is expected that geometric effects will dominate any higher-order scattering effects and cross section generation with Serpent 2 may be preferable.

5.1 Future Work

In the future, the work presented here may be extended to more general fast reactor simulations. The first step of this is to investigate the effects of more complex geometries. As for the geometric restrictions in TWODANT, ANL reports that their Method of Characteristics (MOC) neutron transport computer code, PROTEUS, can be used instead of TWODANT in association with MC^2-3 to describe more general reactor geometries. This improvement is expected to be released in a future version of MC^2-3.

Future work may also include the investigation of higher-order neutron scattering in association with the Simplified P_n (SP_N) equations. The SP_N equations are simpler to solve than the neutron transport equation and are often preferred for fast reactor simulations. Incorporation of higher-order neutron scattering into a fast reactor SP_N calculation may offer improved fidelity in a commonly employed, reduced-order reactor model.

Acknowledgments

This work was funded in part under the Nuclear Energy Advanced Modeling and Simulation (NEAMS) program managed by the Department of Energy Office of Nuclear Energy, under DOE Idaho Operations Office Contract DE-AC07-05ID14517. Accordingly, the U.S. Government retains a nonexclusive, royalty-free license to publish or reproduce the published form of this contribution, or allow others to do so, for U.S. Government purposes. This material is also based upon work supported under an Integrated University Program Graduate Fellowship.

Acronyms

ANL Argonne National Laboratory.
BG Broad Group.
INL Idaho National Laboratory.
LWR light water reactor.
MOC Method of Characteristics.
pcm percent-mille (10^{-5}).
SFR sodium-cooled fast reactor.
SP_N Simplified P_n.
SPH SuPer Homogenization.
TCP0 transport-corrected P_0.
UFG Ultrafine Group.

References

[1] C. H. Lee and W. S. Yang. *MC2-3: Multigroup Cross Section Generation Code for Fast Reactor Analysis*. Tech. rep. ANL/NE-11-41. Argonne National Laboratory, 2012.

[2] L. Cai. "Condensation and Homogenization of Cross Sections for the Deterministic Transport Codes with the Monte Carlo Method: Application to the GEN IV Fast Neutron Reactors." PhD thesis. Université Paris Sud, 2014.

[3] J. Leppänen. "Development of a New Monte Carlo Reactor Physics Code." PhD thesis. Helsinki University of Technology, 2007.

[4] E. Redmond II. "Multigroup Cross Section Generation Via Monte Carlo Methods." PhD thesis. Massachusetts Institute of Technology, 1997.

[5] J. J. Duderstadt and L. J. Hamilton. *Nuclear Reactor Analysis*. New York: John Wiley & Sons, Inc., 1976.

[6] G. Chiba. "Effect of Neutron Anisotropic Scattering in Fast Reactor Analysis." In: *Transactions of the Atomic Energy Society of Japan* 3.2 (2004), pp. 200–207.

[7] J. Ortensi et al. "A Newton Solution for the Superhomogenization Method: The PJFNK-SPH." In: *Annals of Nuclear Energy* 111 (2018), pp. 579–594.

[8] V. Labouré et al. "Hybrid Super Homogenization and Discontinuity Factor Method for Continuous Finite Element Diffusion." In: *Annals of Nuclear Energy* 128 (2019), pp. 443–454.

[9] *ENDF-6 Formats Manual*. Tech. rep. BNL-90365-2009. Brookhaven National Laboratory, July 2010.

[10] M. Asgari. "Development of a New Method for Particle Transport Calculations Utilizing Pointwise-Continuous Nuclear Data." PhD thesis. Louisiana State University, 1998.

[11] J. Leppänen et al. "The Serpent Monte Carlo Code: Status, Development, and Applications in 2013." In: *Annals of Nuclear Energy* 82 (Aug. 2015), pp. 142–150.

[12] *MCNP Users Manual - Code Version 6.2*. Tech. rep. LA-UR-17-29981. Los Alamos National Laboratory, 2017.

[13] R. E. Alcouffe et al. *DANTSYS: A Diffusion Accelerated Neutral Particle Transport Code System*. Tech. rep. LA-12969-M. Los Alamos National Laboratory, June 1995.

[14] J. Leppänen. Private Communication. 2019.

[15] Y. Wang, S. Schunert, and V. Labouré. *Rattlesnake Theory Manual*. Tech. rep. INL/EXT-17-42103. Idaho National Laboratory, Apr. 2019.

[16] J. K. Fink and L. Leibowitz. *Thermodynamic and Transport Properties of Sodium Liquid and Vapor*. Tech. rep. ANL/RE-95/2. Argonne National Laboratory, 1995.

[17] Y. Chen. "Irradiation Effects of HT-9 Martensitic Steel." In: *Nuclear Engineering and Technology* 45.3 (2013), pp. 311–322.

[18] J. C. Wagner, E. L. Redmond, S. P. Palmtag, and J. S. Hendricks. *MCNP: Multigroup/Adjoint Capabilities*. Tech. rep. LA-12704. Los Alamos National Laboratory, Apr. 1994.

[19] G. I. Bell, G. E. Hansen, and H. A. Sandmeier. "Multitable Treatments of Anisotropic Scattering in S_N Multigroup Transport Calculations." In: *Nuclear Science and Engineering* 28.3 (1967), pp. 376–383.

A Material Compositions

All materials listed are present in the ENDF/B-VII.0 library. All cross sections are tabulated at a temperature of 300 K.

Table A.1: Fuel Material Number Densities for U-10Zr with 10 wt.% ^{235}U.

Nuclide	ZAID	MC^2-3	Density $\frac{1}{\text{barn}\cdot\text{cm}}$
^{235}U	92235	U235_7	3.643269×10^{-3}
^{238}U	92238	U238_7	3.237526×10^{-2}
^{90}Zr	40090	ZR90_7	5.366310×10^{-3}
^{91}Zr	40091	ZR91_7	1.170262×10^{-3}
^{92}Zr	40092	ZR92_7	1.788770×10^{-3}
^{94}Zr	40094	ZR94_7	1.812759×10^{-3}
^{96}Zr	40096	ZR96_7	2.920441×10^{-4}

Table A.2: Sodium Material Number Density.

Nuclide	ZAID	MC^2-3	Density $\frac{1}{\text{barn}\cdot\text{cm}}$
^{23}Na	11023	NA23_7	4.644867×10^{-2}

Table A.3: HT9 Stainless Steel Material Number Densities.

Nuclide	ZAID	MC^2-3	Density $\frac{1}{\text{barn}\cdot\text{cm}}$
^{50}Cr	24050	CR50_7	4.861123×10^{-4}
^{52}Cr	24052	CR52_7	9.374191×10^{-3}
^{53}Cr	24053	CR53_7	1.062958×10^{-3}
^{54}Cr	24054	CR54_7	2.645927×10^{-4}
^{92}Mo	42092	MO92_7	7.499119×10^{-5}
^{94}Mo	42094	MO94_7	4.674316×10^{-5}
^{95}Mo	42095	MO95_7	8.044877×10^{-5}
^{96}Mo	42096	MO96_7	8.428929×10^{-5}
^{97}Mo	42097	MO97_7	4.825915×10^{-5}
^{98}Mo	42098	MO98_7	1.219365×10^{-4}
^{100}Mo	42100	MO1007	4.866342×10^{-5}
^{182}W	74182	W182_7	3.509658×10^{-5}
^{183}W	74183	W183_7	1.886672×10^{-5}
^{184}W	74184	W184_7	4.039666×10^{-5}
^{186}W	74186	W186_7	3.748294×10^{-5}
^{58}Ni	28058	NI58_7	2.811366×10^{-4}
^{60}Ni	28060	NI60_7	1.082933×10^{-4}
^{61}Ni	28061	NI61_7	4.707436×10^{-6}
^{62}Ni	28062	NI62_7	1.500937×10^{-5}
^{64}Ni	28064	NI64_7	3.822443×10^{-6}
V	23000	V____7	2.378942×10^{-4}
C	6000	C____7	8.078776×10^{-4}
^{54}Fe	26054	FE54_7	4.340659×10^{-3}
^{56}Fe	26056	FE56_7	6.813907×10^{-2}
^{57}Fe	26057	FE57_7	1.573628×10^{-3}
^{58}Fe	26058	FE58_7	2.094210×10^{-4}